Helmholtz Hodge decomposition of scalar optical fields

Monika Bahl* and P. Senthilkumaran

Department of Physics, Indian Institute of Technology Delhi, New Delhi 110016, India
**Corresponding author: monikaiitd1@gmail.com*

Received July 27, 2012; accepted September 13, 2012;
posted September 27, 2012 (Doc. ID 173400); published October 22, 2012

It is shown that the vector field decomposition method, namely, the Helmholtz Hodge decomposition, can also be applied to analyze scalar optical fields that are ubiquitously present in interference and diffraction optics. A phase gradient field that depicts the propagation and Poynting vector directions can hence be separated into solenoidal and irrotational components.

OCIS codes: 260.0260, 260.2110, 260.6042, 350.0350, 350.4855.

1. INTRODUCTION

Helmholtz Hodge decomposition (HHD) allows a vector field that is defined in a region Ω on a bounded domain and is twice continuously differentiable to be separated into the divergence-free part (solenoidal) and the curl-free part (irrotational) [1–9]. It has been used in the solution of many problems in electromagnetism, MRI data analysis [6], and fluid and smoke simulations [7]. HHD helps in representing the homogeneous data explicitly and visualizing and extracting the critical points like sources, sinks, and vortices. In optics, it has been suggested for vector fields [8] that include polarization and in-phase reconstruction problems to correct wavefront distortions [9]. So far, there are no reports on the use of HHD on scalar optical fields, which, per se, are manifest in the diffraction and interference phenomenon.

Orbital angular momentum (OAM) in scalar optical fields is related to its phase and amplitude distributions [10]. The vectorial nature that is due to the polarization of the wave is disregarded in such fields. We show the usefulness of the HHD in analyzing all such fields, including the ones obtained in interference optics where a single state of polarization is assumed.

We first construct a phase gradient field $\nabla\phi$ from a scalar field [11,12] by using the relation

$$\nabla\phi = \frac{\mathrm{Im}[\psi^*\nabla\psi]}{I}, \tag{1}$$

where ψ is a scalar field resulting from interference or diffraction and $I = \psi^*\psi$ is the intensity distribution.

$\nabla\phi$ points in the direction of the local propagation vector that is normal to the phase contour surfaces. The phase gradient fields in a singular beam can be seen to have a nonzero curl [13–21]. Hence, the solenoidal part that is an explicit component of HHD carries the circulating internal energy of the field. The irrotational part is then devoid of singularities and depicts the spreading of optical energy.

The HHD technique and the method adopted for decomposition is addressed in the next section. Henceforth, the technique is applied on a spherical beam to verify the approach, and then it is applied onto random fields in which both positive and negative curvatures are added. In a spherical wave, the transverse phase gradient has either a positive or a negative divergence, while a random wavefront containing optical vortices exhibits a rotational phase gradient. As a third example, an interference field formed by the superposition of plane waves in the generation of vortex lattices [22–24] is investigated. It is envisaged that the solenoidal part of singular optical fields carries a higher degree of internal circulating energy and, hence, would yield better functionality when used for applications as in tweezer traps, micromachines, and spanners. The irrotational term is devoid of any singularities and can be used as a vortex free field, wherever required. We believe that this method will augment the flow visualization of velocity, pressure and temperature using optical methods [25].

2. HELMHOLTZ HODGE DECOMPOSITION

The HHD is based on the Helmholtz theorem [26], which states that a vector field F that is on a bounded domain V in $\mathbf{R}^3$ and is twice continuously differentiable and whose divergence $\nabla\cdot F = b(r)$ and curl $\nabla\times F = c(r)$ are known can be [2–4] segregated into components f_1 and f_2, determined by

$$F = f_1 + f_2 \Rightarrow \nabla\varphi + \nabla\times A, \tag{2}$$

where $\varphi(r)$ and $A(r)$ are scalar and vector potentials, respectively, that can be obtained from Poisson's equations [26]

$$\varphi(r) = \frac{1}{4\pi}\int_V \frac{b(r)}{r}\,\mathrm{d}v', \tag{3}$$

$$A(r) = \frac{1}{4\pi}\int_V \frac{c(r)}{r}\,\mathrm{d}v'. \tag{4}$$

These potentials, $\varphi(r)$ and $A(r)$, allow the field f to be segregated into the curl-free and divergence-free components.

The boundary conditions imposed in HHD ensure a normal boundary flow on the curl-free component and a tangential flow on the divergence-free component [5]. Considering $\hat{n}$ as the outward normal to the boundary Ω, this implies that for a unique decomposition

(a) the irrotational component f_1 is normal to the boundary $d\Omega$ of Ω, i.e., $\vec{f}_1\times\hat{n} = 0$, and

(b) the solenoidal component f_2 is parallel to the boundary $d\Omega$ of Ω, i.e., $\vec{f}_2 \cdot \hat{n} = 0$.

The method adopted [27] to solve the HHD problem involves minimizing the errors in the terms that are constructed from the initial guesses. f_1 and f_2 are considered as the initial guesses for the curl-free and the divergence-free component fields of a vector field f.

The error terms/residuals $\|\nabla \times f_1\|$, $\|\nabla \cdot f_2\|$ and $\|f_1 + f_2 - f\|$ are then reduced to a minimum.

In a Cartesian coordinate system, the difference operator operating on a scalar function, f, is defined as

$$d\vec{f} = \frac{\partial f_x}{\partial x}\hat{x} + \frac{\partial f_y}{\partial y}\hat{y} + \frac{\partial f_z}{\partial z}\hat{z}. \tag{5}$$

Using finite difference approximation [27,28], the ∂ operator can be written as a matrix given by

$$\partial = \frac{1}{2}\begin{bmatrix} 0 & -1 & 0 & \cdots & 0 \\ 1 & 0 & -1 & \ddots & \vdots \\ 0 & 1 & 0 & \ddots & 0 \\ \vdots & \ddots & \ddots & \ddots & -1 \\ 0 & \cdots & 0 & 1 & 0 \end{bmatrix}. \tag{6}$$

This is true for 1D but for 3D it is expanded as [27]

$$\partial_{x,3D} = I_m \otimes I_m \otimes \partial_x \approx \partial_x, \tag{7}$$

where I_m is an $m \times m$ Identity matrix and $\otimes$ is the Kronecker delta product. Similarly,

$$\partial_{y,3D} = I_m \otimes \partial_y \otimes I_m \approx \partial_y, \tag{8}$$

$$\partial_{z,3D} = \partial_z \otimes I_m \otimes I_m \approx \partial_z. \tag{9}$$

The curl, in the Cartesian coordinate system, is written using the finite difference operator matrix as

$$\nabla \times f = \begin{bmatrix} \hat{x} & \hat{y} & \hat{z} \\ \frac{\partial}{\partial x} & \frac{\partial}{\partial y} & \frac{\partial}{\partial z} \\ f_x & f_y & f_z \end{bmatrix} = \begin{bmatrix} 0 & -\partial_z & \partial_y \\ \partial_z & 0 & -\partial_x \\ -\partial_y & \partial_x & 0 \end{bmatrix}\begin{bmatrix} f_x \\ f_y \\ f_z \end{bmatrix}. \tag{10}$$

Similarly, for divergence,

$$\nabla \cdot f = \frac{\partial f_x}{\partial x} + \frac{\partial f_y}{\partial y} + \frac{\partial f_z}{\partial z} = \begin{bmatrix} \partial_x & \partial_y & \partial_z \end{bmatrix}\begin{bmatrix} f_x \\ f_y \\ f_z \end{bmatrix}. \tag{11}$$

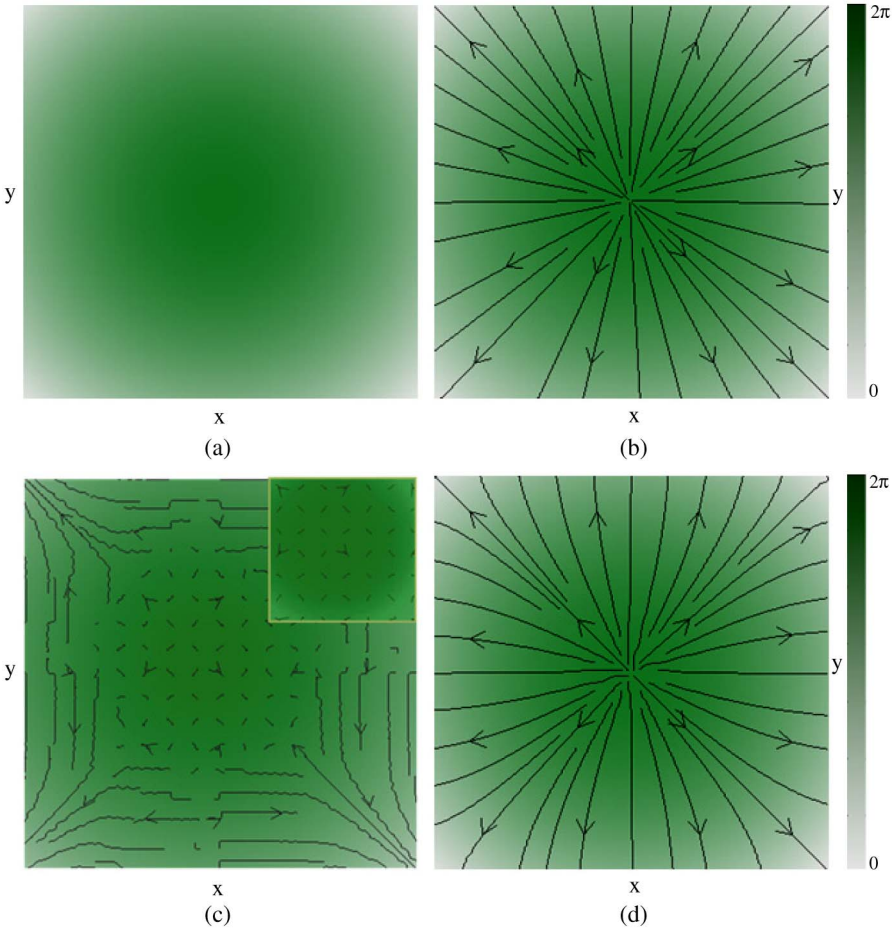

Fig. 1. (Color online) HHD of a spherical beam with positive divergence. (a) Transverse (x-y plane) phase profile for a spherical beam with a positive curvature. The smooth variation of color from green to white depicts the shape of the wavefront. The phase distribution has maxima at the center and decreases toward the boundaries, rendering it a spherical wavefront with a positive divergence. (b) Phase gradient field lines of the beam superimposed on the phase profile. (c) Flow lines of the solenoidal component of the Hodge decomposed field. Inset, magnified view of the beam near the center. (d) Irrotational component with field lines diverging from the center.

Thus, the HHD can then be summarized as

$$\begin{bmatrix} 0 & -\partial_z & \partial_y & 0 & 0 & 0 \\ \partial_z & 0 & -\partial_x & 0 & 0 & 0 \\ -\partial_y & \partial_x & 0 & 0 & 0 & 0 \\ 0 & 0 & 0 & \partial_x & \partial_y & \partial_z \\ I & 0 & 0 & I & 0 & 0 \\ 0 & I & 0 & 0 & I & 0 \\ 0 & 0 & I & 0 & 0 & I \end{bmatrix} \begin{bmatrix} f_{1x} \\ f_{1y} \\ f_{1z} \\ f_{2x} \\ f_{2y} \\ f_{2z} \end{bmatrix} = \begin{bmatrix} 0 \\ 0 \\ 0 \\ 0 \\ f_x \\ f_y \\ f_z \end{bmatrix}. \quad (12)$$

The boundary condition considered is that the fields tend to go to zero at infinity. By applying the abovementioned boundary conditions, the system of equations can be efficiently solved. Equation (12) can be solved as an equation of the form $Px = Q$ where P represents

$$\begin{bmatrix} 0 & -\partial_z & \partial_y & 0 & 0 & 0 \\ \partial_z & 0 & -\partial_x & 0 & 0 & 0 \\ -\partial_y & \partial_x & 0 & 0 & 0 & 0 \\ 0 & 0 & 0 & \partial_x & \partial_y & \partial_z \\ I & 0 & 0 & I & 0 & 0 \\ 0 & I & 0 & 0 & I & 0 \\ 0 & 0 & I & 0 & 0 & I \end{bmatrix}, \text{ while } \begin{bmatrix} f_{1x} \\ f_{1y} \\ f_{1z} \\ f_{2x} \\ f_{2y} \\ f_{2z} \end{bmatrix} \text{ and } \begin{bmatrix} 0 \\ 0 \\ 0 \\ 0 \\ f_x \\ f_y \\ f_z \end{bmatrix}$$

are represented by x and Q respectively.

Since the system of equations is not full rank, appropriate weights are applied to the residuals or error terms in order to get a unique solution. The weight parameters α, β, and γ are defined for the curl-free, divergence-free and the sum residual, respectively.

Thus, one minimizes the expression $\|W(Px - Q)\|$, where W is a diagonal matrix defined as

$$W = \text{diag}([\alpha \quad \alpha \quad \alpha \quad \beta \quad \gamma \quad \gamma \quad \gamma]). \quad (13)$$

The results obtained are shown in the next section. One clearly observes the normal component of the field vanishing at the boundaries, as seen in the solenoidal part. Similarly, the tangential component of the field seems to vanish at the boundaries, as is visible in the irrotational part. The boundary conditions imposed ensure a unique and orthogonal decomposition of the original field. The curl-free part is the projection of the original field onto the space of solenoidal fields. Similarly, the divergence-free part is the projection of the original field onto the space of irrotational fields. This is possible only when proper boundary conditions are satisfied.

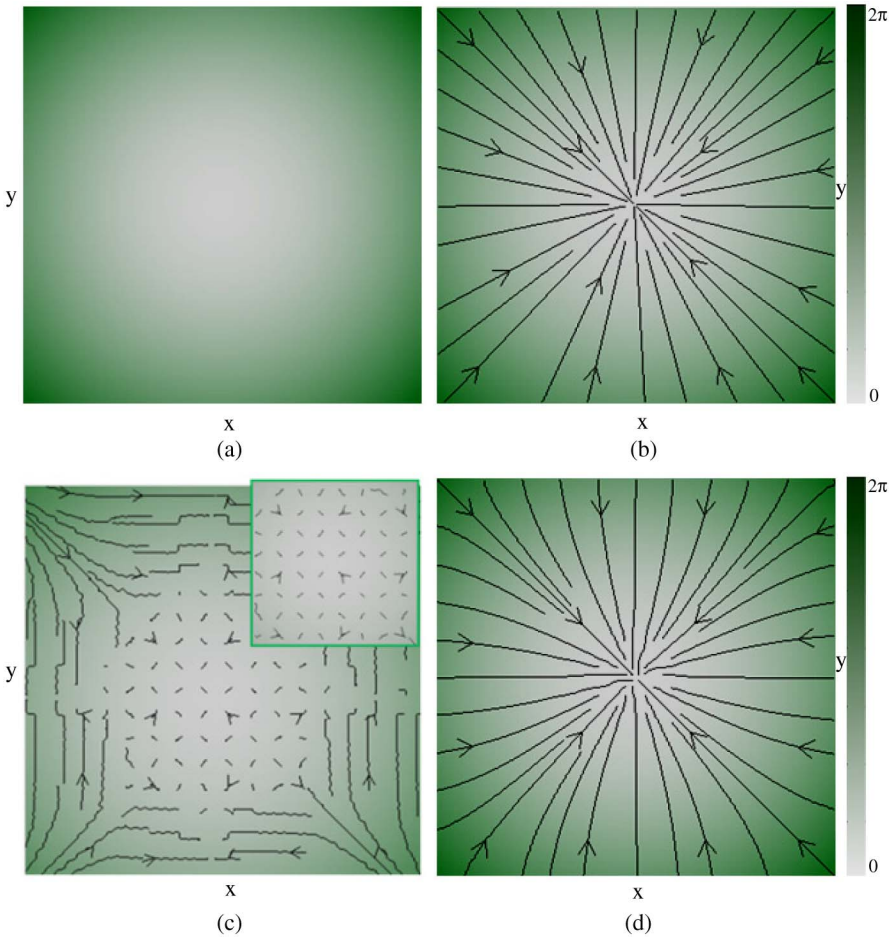

Fig. 2. (Color online) HHD of a spherical beam with negative divergence. (a) Transverse (x-y plane) phase profile for a spherical beam with a negative curvature. The smooth variation of color from white to green depicts the shape of the wavefront. The phase distribution has minima at the center and increases toward the boundaries, thus rendering it a spherical shape with a negative divergence. (b) Phase gradient field lines of the beam superimposed on the phase profile. (c) Flow lines of the solenoidal component of the Hodge decomposed field. Inset, magnified view of the beam near the center. (d) Irrotational component with field lines converging toward the centre.

3. DECOMPOSITION OF SCALAR OPTICAL FIELDS

In this section, the decomposition using HHD method for some of the scalar optical fields is demonstrated. The simulation work has been done using MATLAB.

Under the quadratic approximation, a unit amplitude spherical beam can be represented as $\psi = \exp(ik(x^2 + y^2)/2z_o)$, where z_o represents the axial distance from the point source to the observation plane. Because a spherical beam carries no curl component, it has been considered as the first example for verifying the HHD tool. The phase of the beam is shown in Fig. 1(a). The phase gradient field, as computed by using Eq. (1), is shown in Fig. 1(b). The same can be verified by finding the gradient field mathematically. It is important to note here that Eq. (1) plays a very important role when dealing with phase gradients of optical scalar fields. First, it relates the phase gradient directly to the expression for the field. The first example considered is a spherical beam that has a simple analytical expression for the phase distribution, and, therefore, it is easy to verify the gradient using mathematical treatment. But, in reality, one comes across several stances in diffraction and interference optics, where the phase distributions are not expressed as simple analytical expressions, and hence, finding the phase gradient is a complex task at hand.

Second, the computed phase distributions are usually represented by wrapped phase maps. The 2π phase jumps appear as discontinuities where the gradient field lines reverse in direction. This is not the case in reality and leads to misleading results. Such problems are not encountered when Eq. (1) is used to compute gradients. Thus, the method adopted for HHD works perfectly when operated on optical scalar fields whose gradients are derived in the above mentioned way.

A spherical beam has an explicit divergence component, and this can be seen in the cross sectional plane for the phase gradient field in Fig. 1(b). The background to the field lines in all the figures is the transverse phase distribution. The smooth variation of color from green to white in Fig. 1 depicts the shape of the wavefront. The phase distribution has maxima at the center and decreases toward the boundaries. This is the spherical wavefront with a positive divergence. One observes the field streamlines diverging from the central core in Fig. 1(b). Figure 1(c) shows the Hodge decomposed divergence-free part. As can be seen, the solenoidal field is zero in the core area far away from the boundary. The normal component of the field vanishes near the boundary, and the field lines tend to get parallel here. The irrotational component shows diverging field lines emanating from the center, as

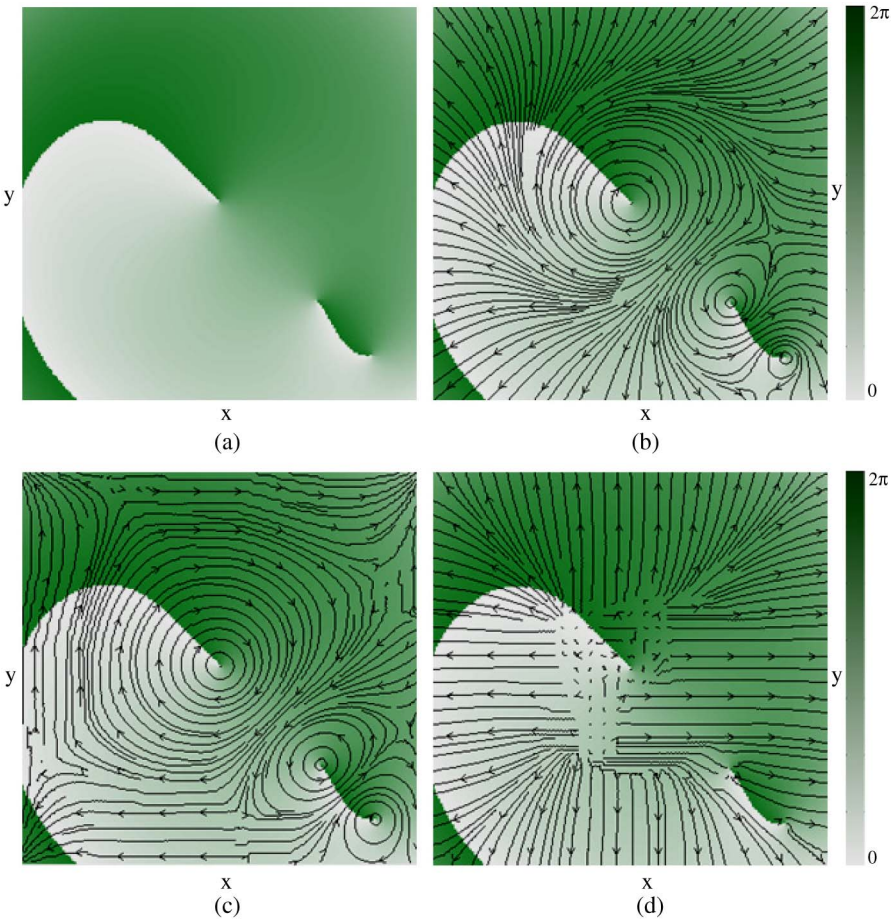

Fig. 3. (Color online) HHD of a random vortex field added to a positively diverging spherical beam. (a) Transverse phase profile of a random vortex field added to a spherical beam with a positive curvature. The smooth variation of color from green to white in the background shows that the phase distribution has maxima at the center and reduces toward the boundaries exhibiting a positive divergence. (b) Phase gradient field lines of the beam superimposed on the phase profile. (c) Flow lines of the solenoidal component of the Hodge decomposed field. The field lines circulate about the vortex centers. (d) Irrotational component with diverging field lines. This is the vortex free field.

shown in Fig. 1(d). As expected, the normal component tends to be perpendicular at all points on the boundary. A similar example is considered for a spherical beam with a negative divergence. The smooth variation of color from white to green in Fig. 2 depicts the shape of the wavefront. The phase distribution has minima at the center and increases toward the boundaries, thus rendering it a spherical shape with a negative divergence. Figure 2(a) shows the transverse phase profile of the beam. Figure 2(b) depicts the field lines converging to the centre. Figures 2(c) and 2(d) show the Hodge decomposed fields. The curl-free part in both the abovementioned examples is devoid of any rotational features, as can be seen in Figs. 1(c) and 2(c). We thus visualize that the OAM, which is associated with the circulating phase, is explicitly absent, en masse, in a spherical wave.

Speckle fields are known to contain vortices. A random field with embedded vortices is considered as a second example. A positive/negative curvature that introduces a positively/negatively diverging gradient is added to the former curling gradient field. Thus, both the curl and divergence components are manifested in it. Figures 3 and 4 show the HHD decomposed scalar fields. Figures 3(a) and 4(a) show the phase maps of the original fields. Figures 3(b) and 4(b) show the stream lines of the fields superposed on the phase profiles of the beams. As can be seen in Figs. 3(c) and 4(c), these vortex singularities are extracted out in the divergence free component. The curl-free part, as in Figs. 3(d) and 4(d), is completely devoid of them and shows diverging/converging field lines, depicting clearly the curvature of the superposed spherical beam. This is the vortex-free field. We envisage that HHD can, hence, be used to produce speckle free fields wherever required.

In the third example, a real life experimental result is modeled as an original field for decomposition [23]. This is the structured optical vortex lattice field. It is noteworthy that a plane wave does not carry any vortex but when three or more such waves interfere, the resultant field shows vortices embedded in a lattice. One such lattice field is considered here that has been constructed by a superposition of three plane waves. The transverse phase map of the vortex distribution, with the intensity profile in the inset, is shown in Fig. 5(a). Figures 5(c) and 5(d) show the Hodge decomposed lattice field. As expected, the solenoidal part seen in Fig. 5(c) carries all the curl features from the original field. The phase gradient contours circulate about the vortex centers. The irrotational part as seen in Fig. 5(d) shows web-like gradient field lines

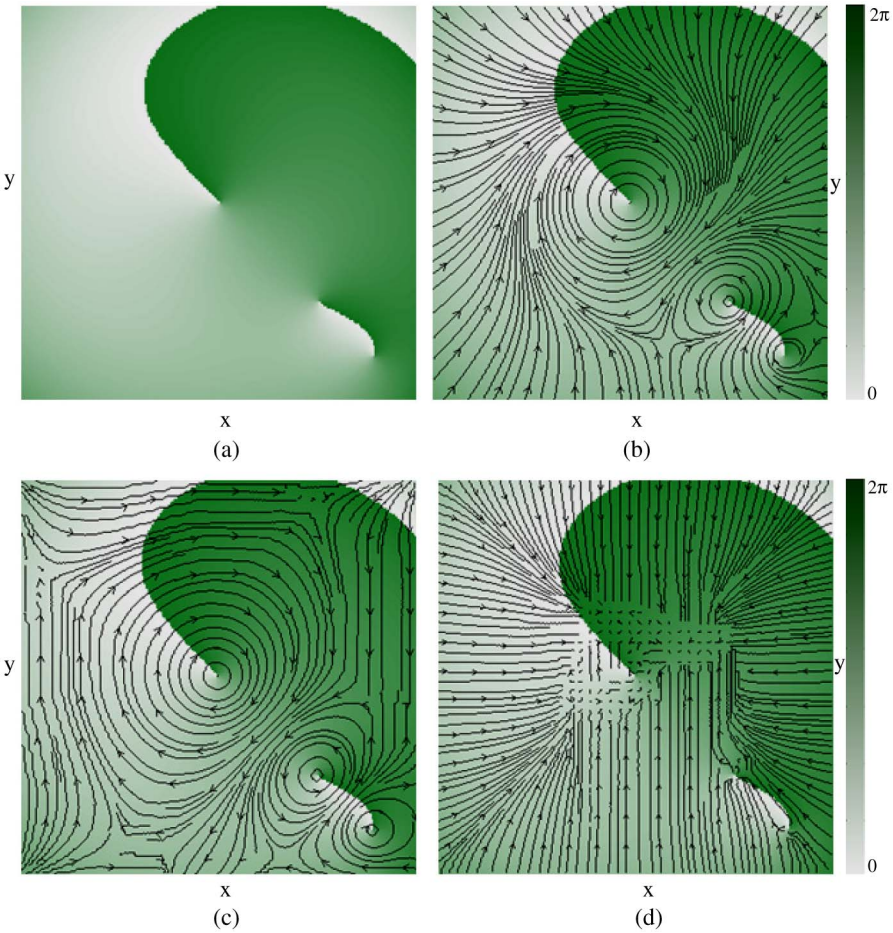

Fig. 4. (Color online) HHD of a random vortex field added to a negatively diverging spherical beam. (a) Transverse phase profile of a random vortex field added to a spherical beam with a negative curvature. The smooth variation of color from white to green in the background shows that the phase distribution has minima at the center and increases toward the boundaries exhibiting a negative divergence. (b) Phase gradient field lines of the beam superimposed on the phase profile. (c), (d) Represent the Hodge decomposed field. (c) Flow lines of the solenoidal component of (b). The field lines circulate about the vortex centers. (d) Irrotational component with converging field lines. This is the vortex-free field.

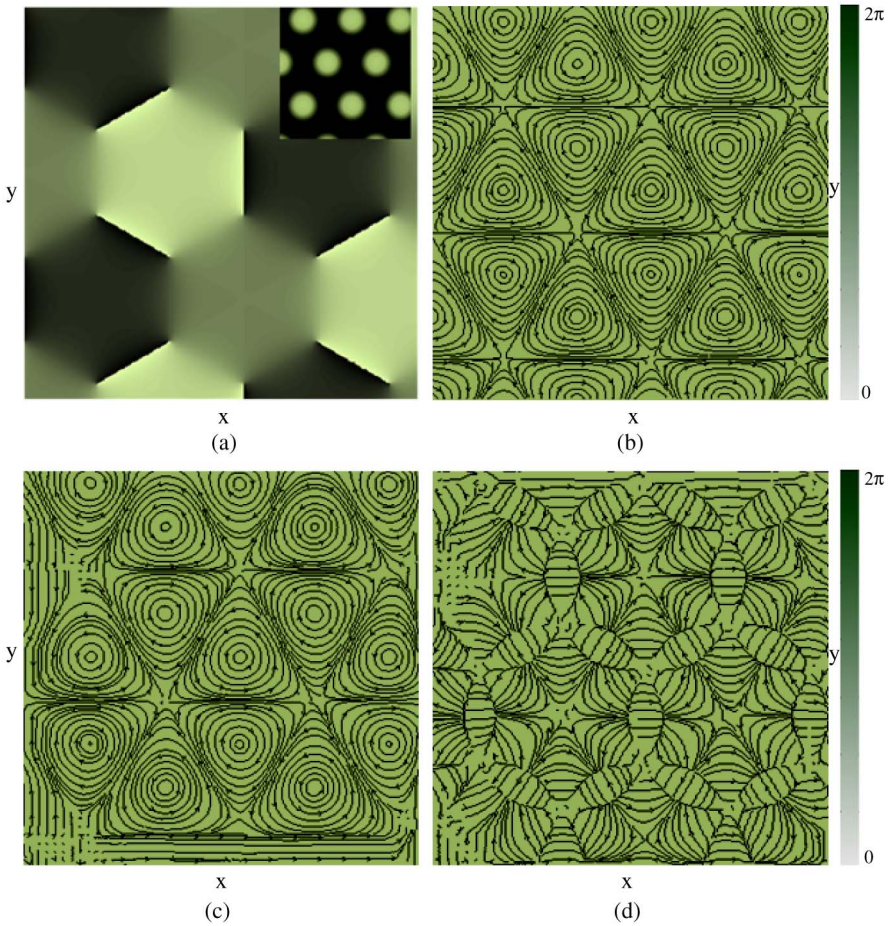

Fig. 5. (Color online) HHD for a three beam interference pattern. (a) Transverse phase profile of the original field. Inset, cross-sectional view of the intensity profile in the x-y plane. (b) Phase gradient field lines of the corresponding pattern. (c), (d) Represent the Hodge decomposed vortex lattice field. (c) Phase gradient field lines of the extracted solenoidal component of (b). (d) Irrotational component with flow lines forming a web-like pattern.

about the singularities. This is the vortex free field. This can be used in optics where a vortex free field is required or discarded as a noise term.

There is no method reported so far for segregating the curl-free and the divergence-free components for optical scalar fields. This paper illustrates the same using the HHD technique. HHD applied to an interference field has also been demonstrated. One can, on similar lines, decompose any field obtained in interference/diffractive optics, and study its propagation dynamics and other topological features.

4. CONCLUSIONS

We have established that HHD, which has been, hitherto, applied only to vector fields, can also be used as a tool to analyze scalar optical fields. Such fields are ubiquitous in diffraction and interference optics. We have demonstrated that the HHD can be dexterously applied to them, and the solenoidal and irrotational components can be efficiently segmented. This has been solved in the rectangular coordinate system with general boundary conditions. The propagation of optical beams in circular cross-sectional channels is also of interest. The HHD method described above would also yield important results in the study of propagation of optical beams. The segregated component fields would give a lot of insight into the generation and annihilation of optical vortices during propagation. This is currently under investigation and shall be produced in a later work. As already stated, the OAM, and hence the Poynting vector, is directly related to the phase gradient of these fields. We envisage that in the case of singular optical fields, the solenoidal part carries a higher degree of internal circulating energy and hence, can be separated out from the irrotational part. The former component, when used directly for applications as in tweezer traps, micromachines, spanners, etc., would yield better functionality. The latter term, which is curl free, is sometimes regarded as the noise term and hence, can be discarded. This is also the component that is devoid of any singularities and can, therefore, be used as a vortex free field wherever required. We believe that the HHD will also augment the flow visualization using optical methods [25] for several other fields including velocity, pressure and temperature.

REFERENCES

1. A. Globus, C. Levit, and T. Lasinki, "A tool for visualizing the topology of three-dimensional vector fields," in *Proceedings of IEEE on Visualization* (IEEE, 1991), pp. 33–40.
2. K. Polthier and E. Preuss, "Identifying vector field singularities using a discrete Hodge decomposition," in *Visualization and Mathematics III*, H. C. Hege and K. Polthier, eds. (Springer Verlag, 2002), pp. 113–134.

3. Y. Tong, S. Lombeyda, A. N. Hirani, and M. Desbrun, "Discrete multiscale vector field decomposition," ACM Trans. Graph. **22**, 445–452 (2003).
4. F. Petronetto, A. Paiva, M. Lage, G. Tavares, H. Lopes, and T. Lewiner, "Meshless Helmholtz-Hodge decomposition," IEEE Trans. Vis. Comput. Graphics **16**, 338–342 (2010).
5. F. M. Denaro, "On the application of the Helmholtz–Hodge decomposition in projection methods for incompressible flows with general boundary conditions," Int. J. Numer. Methods Fluids **43**, 43–69 (2003).
6. I. Kaya, A. P. Santhanam, C. Imielinska, and J. Rolland, "Modeling air-flow in the tracheobronchial tree using computational fluid dynamics," in *Proceedings of 2007 MICCAI Workshop on Computational Biomechanics* (2007), pp. 142–151.
7. R. Fedkiw, J. Stam, and H. W. Jensen, "Visual simulation of smoke," in *Proceedings of ACM SIGGRAPH 2001*, *Proceedings of the 28th Annual Conference on Computer Graphics and Interactive Techniques*, Eugene Fiume, ed. (Association for Computing Machinery, 2001), pp. 15–22.
8. A. M. Stewart, "Angular momentum of light," J. Mod. Opt. **52**, 1145–1154 (2005).
9. M. Hattori and S. Komatsu, "An exact formulation of a filter for rotation in phase gradients and its applications to wavefront reconstruction problems," J. Mod. Opt. **50**, 1705–1723 (2003).
10. G. Molina-Terriza, J. P. Torres, and L. Torner, "Twisted photons," Nat. Phys. **3**, 305–310 (2007).
11. M. Berry, "Optical currents," J. Opt. A **11**, 1464–1475 (2009).
12. M. Born and E. Wolf, *Principles of Optics* (Cambridge University, 2002).
13. L. Allen and M. J. Padgett, "The Poynting vector in Laguerre Gaussian beams and the interpretation of their angular momentum density," Opt. Commun. **184**, 67–71 (2000).
14. L. Allen, M. W. Beijersbergen, R. J. C. Spreeuw, and J. P. Woerdman, "Orbital angular momentum of light and the transformation of Laguerre-Gaussian laser modes," Phys. Rev. A **45**, 8185–8189 (1992).
15. S. F. Arnold, L. Allen, and M. Padgett, "Advances in optical angular momentum," Laser Photon. Rev. **2**, 299–315 (2008).
16. M. Padgett and L. Allen, "Optical tweezers and spanners," Phys. World **10**, 35–38 (1997).
17. M. S. Soskin and M. V. Vasnetsov, "Singular optics," Prog. Opt. **42**, 219–276 (2001).
18. A. M. Yao and M. J. Padgett, "Orbital angular momentum: origins, behavior and applications," Adv. Opt. Photon. **3**, 161–204 (2011).
19. I. V. Basistiy, M. S. Soskin, and M. V. Vasnetsov, "Optical wavefront dislocations and their properties," Opt. Commun. **119**, 604–612 (1995).
20. I. V. Basistiy, V. Y. Bazhenov, M. S. Soskin, and M. V. Vasnetsov, "Optics of light beams with screw dislocations," Opt. Commun. **103**, 422–428 (1993).
21. P. Senthilkumaran, F. Wyrowski, and H. Schimmel, "Vortex stagnation problem in iterative Fourier transform algorithms," Opt. Lasers Eng. **43**, 43–56 (2005).
22. S. Vyas and P. Senthilkumaran, "Interferometric optical vortex array generator," Appl. Opt. **46**, 2893–2898 (2007).
23. J. Xavier, S. Vyas, P. Senthilkumaran, and J. Joseph, "Tailored complex 3D vortex lattice structures by perturbed multiples of three-plane waves," Appl. Opt. **51**, 1872–1878 (2012).
24. D. P. Ghai, S. Vyas, P. Senthilkumaran, and R. S. Sirohi, "Vortex lattice generation using interferometric techniques based on lateral shearing," Opt. Commun. **282**, 2692–2698 (2009).
25. J. P. Prenel and D. Ambrosini, "Flow visualization and beyond," Opt. Lasers Eng. **50**, 1–7 (2012).
26. G. B. Arfken and H. J. Weber, *Mathematical Methods for Physicists* (Elsevier, 2005).
27. T. McGraw, T. Kawai, I. Yassine, and L. Zhu, "Visualizing high-order symmetric tensor field structure with differential operators," J. Appl. Math. **2011**, 1–27 (2011).
28. Finite difference method, http://en.wikipedia.org/wiki/Finite_difference_method.